A multiscale, asymptotic model for the subgrid scale stresses in the large-eddy simulation of an incompressible fluid

By A. Novikov† and D. J. Bodony

1. Motivation and objectives

In the development of large-eddy simulation (LES) two primary assumptions are made. The first is that a turbulent flow can be categorized by a hierarchy of lengthscales. For example the largest lengthscales are often associated with the geometry of the flow that, in turn, provide energy to the smaller 'energy containing' lengthscales. Vortex stretching and similar flow processes generate continually smaller lengthscales in the so-called 'inertial range' until the viscosity-controlled limit is reached. This view of turbulence has been evidenced by experimental and numerical data for many years. The second assumption, based primarly on the observations and deductions of Kolmogorov (1941) and emphasized by Batchelor (1953), states that the inertial range is independent of the geometry-controlled scales and viscosity. This isolation leads, in terms of dimensional analysis, to a range of lengthscales with a specific spectral power law (the $-5/3$ law for the three-dimensional energy spectrum). Moreover, the second assumption has influenced how the inerial range turbulence is viewed. Namely, the inertial range supports a cascade wherein energy organized on the scale of the geometry is transferred to, and dissipated as heat by, the viscosity-determined lengthscales.

Supposition of the inertial range to be more associated with energy transport than possessing of a unique signature (in terms of being dependent on the overall flow geometry) has led, in the context of LES, to a series of subgrid scale models that attempt to account for the energy transfer through the inertial range as an effective 'energy sink' in the motion of the larger lengthscales. The Smagorinsky model (Smagorinsky 1963), its dynamic variation (Germano et al. 1991), and the scale-similarity model (Bardina et al. 1980) are based on the statistical homogeneity assumption of the inertial range. (For the many other subgrid scale models see, for example, the review by Meneveau & Katz (2000).) It has been found, however, that the assumptions made in the aforementioned eddy viscosity models limit their response to changes in the flow where, for example, energy is transfered from the small to the large scales (termed backscatter) (Meneveau & Katz 2000). In those cases where backscatter is important, the eddy viscosity models are often too diffusive. By contrast, the scale similarity model is not diffusive enough. Even in homogeneous, isotropic turbulence, backscatter has significance (Meneveau 1991).

In this article, we treat the assumption of statistical homogeneity differently by performing a perturbation analysis of homogeneous, isotropic turbulence computed by direct numerical simulation. The basic idea may be stated as follows: Supposing that the inertial range isolation argument holds true and that one can phenemologically model the inertial range as homogeneous isotropic turbulence, then it should be possible to determine the

† Department of Mathematics, Pennsylvania State University, University Park, PA

effective response of the inertial range turbulence to perturbations in the flow with larger lengthscales. In other words, a charactization or model of the subgrid scale fluctuations is sought that is based not on an *a priori* assumption about the inertial range but that is deduced from the structure of isotropic turbulence.

Treating the subgrid scale field as incompressible, homogeneous, isotropic, turbulence even when the larger scale field is compressible and anisotropic, appears to be a reasonable assumption for low to moderately compressible flows, such as the Mach 1.2 mixing layer analyzed by Bodony & Lele (2002). In that study, it was found that the bulk of the compressibility was carried by the large scale motions up to the dominant energy containing lengthscale. Moreover, the anisotropy associated with the shear layer was also limited to the larger lengthscales, leaving a nascent inertial range scaling of the three-dimensional energy spectrum proportional to $k^{-5/3}$ for $k = |\vec{k}|$, the amplitude of the wavenumber vector. The assumption of isotropic turbulence necessarily limits the relevance of these conclusions to those cases where the Kolmogorov assumption is reasonable.

The use of scale-specific information in deriving a subgrid scale model is not new. Debussche et al. (1993) used a Fourier decomposition to derive approximate equations for motion below a dynamically-determined large-scale/small-scale cut-off wavenumber in their nonlinear Galerkin method. In the wavelet context, Zimin & Hussain (1995) derived a subgrid scale model that permits backscatter and has k^4 and $k^{-5/3}$ scalings in the low- and inertial ranges of wavenumbers, respectively. A wavelet-based analysis of homogeneous isotropic turbulence was conducted by Meneveau (1991), wherein the importance of backscatter and locality in position as well as in scale were highlighted. For the simulation of two-dimensional flows, Laval et al. (2000) developed a dynamic subgrid scale model based on the Gabor transform, which is similar to the continuous wavelet transform. A three-dimensional model applicable to planar channel flows was developed by Dubrulle et al. (2001).

The approach taken here is motivated by the two-scale models of turbulent transport (see, for example, Frisch (1995); Novikov & Papanicolaou (2001); Sivashinsky (1985); Sivashinsky & Frenkel (1992); Sivashinsky & Yakhot (1985)). Therefore, this article is organized first by developing the appropriate multiscale expansions that are needed to isolate the subgrid scale motions from the larger scale motions. The explicit scale separation assumption in the multiscale expansion is then relaxed, and the theory is applied to homogeneous, isotropic turbulence.

2. Derivation of the large- and small-scale equations

It is of interest to describe the response of an incompressible, homogeneous isotropic turbulent field to (possibily anisotropic) large scale perturbations. In the LES modeling context, the large scale field is treated as the LES (resolved) field, and the isotropic turbulence is treated as a model for the subgrid scale field. Only incompressible subgrid scale fields will be considered.

In this spirit, let $v(x,t)$ denote an isotropic turbulent field. Suppose that $v(x,t)$ is given and that it satisfies the incompressible Navier-Stokes equations with forcing f:

$$\frac{\partial}{\partial t}v + v\cdot\nabla v = \frac{1}{Re}\Delta v - \nabla P + f. \tag{2.1}$$

The role of the pressure P in (2.1), as well as in the equations below, is unimportant, so

in reality the Leray projected equation is taken

$$\frac{\partial}{\partial t}v + \mathbb{P}\,(v \cdot \nabla v) = \frac{1}{Re}\Delta v + f, \tag{2.2}$$

where $\mathbb{P}$ is the projection onto a divergence free vector field (see Constantin & Foias (1988)) defined as

$$\mathbb{P}(v) = v - \nabla \cdot \Delta^{-1}(\nabla v).$$

Given the flow v on a finite time interval, say $t \in [t_1, t_2]$, assume that it is perturbed by a large-scale flow $U_o(x)$ at time $t = t_1$. Now require that the perturbed flow $w(x,t)$ also satisfy the Navier-Stokes equations

$$\frac{\partial}{\partial t}w + w \cdot \nabla w = \frac{1}{Re}\Delta w - \nabla P + f \quad \text{subject to} \quad \nabla \cdot w = 0. \tag{2.3}$$

Therefore, initially,

$$w(x, t_1) = v(x, t_1) + U_o(x). \tag{2.4}$$

Then the perturbation $u(x,t) = w(x,t) - v(x,t)$ satisfies

$$\frac{\partial}{\partial t}u + u \cdot \nabla v + v \cdot \nabla u + u \cdot \nabla u = \frac{1}{Re}\Delta u - \nabla P. \tag{2.5}$$

Equation (2.5) characterizes the dynamics of u given any perturbation of v, and its solution is uniquely determined by the initial conditions

$$u(x, t_1) = U_o(x). \tag{2.6}$$

When u is sufficiently small, the solution of (2.5) depends mainly on the underlying *basic flow* $v(x,t)$. Thus, the primary impact on the dynamical properties of u comes from v. In two-scale asymptotics (Frisch 1995; Novikov & Papanicolaou 2001; Novikov 2003; Sivashinsky 1985; Sivashinsky & Frenkel 1992; Sivashinsky & Yakhot 1985), this impact has relevance to the modeling of the Reynolds stress.

The main question of LES modeling stems from the stresses due to large-scale–small-scale interactions and from their dependence on the resolved field. To determine the subgrid scale stresses,

$$u(x,t) = U(x,t) + u'(x,t), \langle u' \rangle = 0$$

is written for the solution of (2.5), where $U(x,t)$ is the "large-scale" and u' is the "small-scale" part of u. The decision as to what should be considered the large and small scales of the flow is delicate, and its discussion is postponed for the moment. Using the standard averaging argument applied to equation (2.5), the large-scale flow satisfies

$$\frac{\partial}{\partial t}U + U \cdot \nabla U + \nabla \cdot \tau = \frac{1}{Re}\Delta U - \nabla P, \tag{2.7}$$

where the Reynolds stress τ is

$$\tau_{ij} = \langle u'_j v_i + v_j u'_i + u'_j u'_i \rangle, \tag{2.8}$$

and the brackets $\langle \cdot \rangle$ denote an average over the small scales, defined below. The goal is to relate τ to the large-scale field U and to the isotropic turbulence v.

2.1. *Two-scale asymptotic expansion*

Under the assumption of separation of scales, the derivation of the effective equation (2.7) and the explicit form of the stress (2.8) can also be given by rigorous asymptotic analysis

(Dubrulle & Frisch 1991; Novikov & Papanicolaou 2001). Let the small parameter ε be the ratio between the dominant wavenumbers of the large and the small scales. Suppose that v is entirely small-scale in nature, that is,

$$v(x,t) = v^\varepsilon(x,t) = v(x,x/\varepsilon,t) = v(x,y,t),\ \ y = x/\varepsilon,$$

and periodic with zero mean in the fast spatial variable $y \in \square \equiv [0,2\pi]^3$:

$$\langle v\rangle(x,t) = \frac{1}{(2\pi)^3}\int_\square v(x,y,t)dy.$$

It is assumed initially that u is solely a large-scale perturbation, i.e. U_o in (2.6) is independent of ε: for any ε, $U_o^\varepsilon(x) \equiv U_o(x)$. Consider, then, the two-scale ansatz (see, for example, Bensoussan et al. (1978))

$$u(x,t) = u^\varepsilon(x,y,t) = U(x,t) + \varepsilon u^1(x,y,t) + \varepsilon^2 u^2(x,y,t) + \ldots, \tag{2.9}$$

where all of the so-called small-scale correctors u^i, $i = 1,2,\ldots$, have zero mean with respect to the fast variable y:

$$\langle u^i\rangle = 0.$$

Using the chain rule, it is obtained that

$$\frac{\partial}{\partial x_i} \equiv \nabla_i = \frac{\partial}{\partial x_i} + \frac{1}{\varepsilon}\frac{\partial}{\partial y_i} \equiv \nabla_i^x + \frac{1}{\varepsilon}\nabla_i^y, \tag{2.10}$$

where ∇_i^x and ∇_i^y are partial derivatives with respect to the slow and the fast spatial variables, respectively. Using (2.9) and (2.10) in the equation for the perturbation (2.5) and then matching asymptotics in ε, the terms of order $1/\varepsilon$ have to satisfy the so-called cell problem for the first corrector

$$\frac{1}{Re}\Delta_y u^1 = \mathbb{P}(U\cdot\nabla^y v). \tag{2.11}$$

The solution to this equation is easily found to be

$$u^1 = Re\,\Delta_y^{-1}\mathbb{P}(U\cdot\nabla^y v), \tag{2.12}$$

where it is verified *a posteriori* that u^1 has, indeed, zero mean. Matching the terms of order ε^0, it is found that

$$\frac{1}{Re}\Delta_y u^2 = \mathbb{P}\left(-\partial_t U - U\cdot\nabla^x U + \frac{1}{Re}\Delta_x U\ - u^1\cdot\nabla^y v \right.$$
$$\left. - v\cdot\nabla^y u^1 - \frac{2}{Re}\nabla^x\nabla^y u^1 - v\cdot\nabla^x U\right). \tag{2.13}$$

Equation (2.13) is solvable in y if the following solvability condition is satisfied:

$$\partial_t U + \mathbb{P}(U\cdot\nabla^x U) + \mathbb{P}(\langle u^1\cdot\nabla^y v + v\cdot\nabla^y u^1\rangle) = \frac{1}{Re}\Delta_x U. \tag{2.14}$$

The solvability condition (2.14) for the zeroth order cell problem determines $U(x,t)$ as a solution of a differential equation for which the fast variable y is eliminated by averaging. This equation is the large-scale equation for $U(x,t)$, as in (2.7), where the term

$$\nabla\cdot\tau = \langle u^1\cdot\nabla^y v + v\cdot\nabla^y u^1\rangle$$

is the divergence of the stress (2.8) to order ε. In order to compute τ, it is sufficient to know u^1 and v only.

2.2. *Discussion of the two-scale asymptotics*

To validate the extent to which the two-scale asymptotics can be applied for a general flow, look at the steps made in the previous section.

The first step was to assume that u has a two-scale expansion (2.9). For general flows it is replaced by a general expansion of the form

$$u(x,t) = U(x,t) + u',\ u' = \varepsilon u^1(x,t) + \varepsilon^2 u^2(x,t) + \ldots,\ U(x,t) = \mathcal{O}(\varepsilon) \tag{2.15}$$

In the expansion (2.15) it is assumed that $U(x,t) = \mathcal{O}(\varepsilon)$ because U is treated as a perturbation of v. Hence, the small parameter ε can be introduced in a general setting as the ratio of the enstrophies

$$\varepsilon = \frac{||\nabla U||_{L^2}}{||\nabla v||_{L^2}}. \tag{2.16}$$

If $v = \mathcal{O}(1)$ but is dominated by small-scales and $U = \mathcal{O}(1)$, then (2.16) is consistent with (2.9). If, however, $v = \mathcal{O}(1)$ but has a full spectrum, then (2.16) can be satisfied by choosing $U_o = O(\varepsilon)$. Hence, it can be assumed in (2.15) that

$$\frac{||\nabla u^{i+1}||_{L^2}}{||\nabla u^i||_{L^2}} = \mathcal{O}(1) \tag{2.17}$$

and matching asymptotics can be performed in ε. Then, u^1 satisfies

$$\frac{\partial u^1}{\partial t} + \mathbb{P}\,(v \cdot \nabla U) + \mathbb{P}\,(U \cdot \nabla v) = \frac{1}{Re}\Delta u^1. \tag{2.18}$$

Further simplifications of (2.18) can be made for large wave-numbers of u^1 by neglecting the term $\frac{\partial}{\partial t}u^1$ (see, e.g. Debussche et al. (1993)). It was also shown by Novikov (2003) that in the two-scale expansion

$$\left|\left|\frac{\partial}{\partial t}u^1\right|\right|_{L^2} \Big/ \left|\left|\Delta u^1\right|\right|_{L^2} = \mathcal{O}(\varepsilon^2).$$

Therefore, $\frac{\partial}{\partial t}u^1$ can be neglected:

$$u^1 = Re\,\Delta^{-1}\mathbb{P}\,(U \cdot \nabla v + v \cdot \nabla U)\,. \tag{2.19}$$

The two-scale analysis (cf. (2.12) and (2.19)) also indicates that it is sufficient to consider an even simpler equation,

$$\tilde{u}^1 = Re\,\Delta^{-1}\mathbb{P}\,(U \cdot \nabla v)\,. \tag{2.20}$$

However, both equations (2.20) and (2.19) have the same computational complexity, and therefore from the practical point of view there is no reason to simplify (2.19) to (2.20).

The next step of the two-scale analysis is an approximation of the Reynolds stress

$$\tau_{ij} \approx \tau^o_{ij} \equiv \langle u^1_i v_j\rangle + \langle v_i u^1_j\rangle. \tag{2.21}$$

This last assumption also follows from the general asymptotic expansion (2.17). Equation (2.7), with the approximation (2.21), (2.19), is exactly what is solved for in large-eddy simulations.

It remains to express the y-average $\langle\cdot\rangle$ and the driving isotropic field in an LES context. Spectral methods are used to solve (2.7), (2.21), and (2.19), and thus Fourier-filtering is used at a certain, numerically determined wave-number to determine $\langle\cdot\rangle$. The advantages of Fourier-filtering for spectral numerical methods in the two-scale context are discussed in Novikov (2004).

The extent of applicability of this analogy between two-scale flows and turbulent flows relies on two assumptions: whether the solutions of (2.20), (2.19), and (2.18) differ insignificantly and whether τ^o is significant. Both questions are addressed numerically.

3. Numerical Investigations of simulated decaying turbulence

In this section, the first consideration is the expression for the subgrid scale stress (2.21) and its application in an *a priori* manner to decaying isotropic turbulence.

3.1. *Large scale initial conditions*

To permit a systematic investigation of the response of τ^o of (2.21) to a range of large-scale perturbations, two classes of well known flows are chosen. The choice of these flows is motivated by the fact that for certain combinations of coefficients, canonical flows (e.g. shear flow, strain flow, closed streamline flow) can be constructed analytically. The perturbations are also chosen to have a large-scale structure consistent with the two-scale decomposition.

The following two types of flow configurations will be used: the first are the Beltrami flows, the so-called ABC-flows, given by

$$\begin{aligned} U_o &= B\sin y - C\cos z, \\ V_o &= C\sin z - A\cos x, \\ W_o &= A\sin x - B\cos y. \end{aligned} \tag{3.1}$$

The second class are Taylor-Green, cat's-eye flows

$$\begin{aligned} U_o &= -\sin x\cos y + \delta\cos x\sin y, \\ V_o &= \sin y\cos x - \delta\cos y\sin x, \\ W_o &= 0. \end{aligned} \tag{3.2}$$

Note that a periodic length of 2π has been assumed in these flows. The energy spectrum of Taylor-Green flows and ABC-flows is given in Figs. 3(a) and 4(a), respectively.

Additionally, for Fig. 10 below, a third type of large-scale initial condition is used as follows. In the isotropic turbulence data, the velocity field is Fourier-filtered at $k = 15$ to construct two parts: (i) a large-scale part with $k < 15$ and (ii) a small-scale part with $k \geq 15$. The long-wavelength portion (i) is then used as the initial conditions for the large-scale equation (2.7).

3.2. *Decaying isotropic turbulence*

Here is discussed the flow configuration of decaying homogeneous, isotropic, turbulence. The turbulence was computed using a fully compressible pseudo-spectral code on 64^3 grid points covering a 2π-periodic domain of size $[0, 2\pi]^3$. Nondimensionalization is with respect to the average density ρ_0, the initial speed of sound a_0, and the lengthscale L, which is chosen to provide the desired initial Taylor Reynolds number. The initial conditions consist of a prescribed three dimensional energy spectrum $E(k)$ of

$$E(k) = A(k/k_0)^4 \exp(-2(k/k_0)^2) \tag{3.3}$$

from which the solenoidal velocity components were constructed following Blaisdell et al. (1991). The initial pressure field satisfies the Poisson equation

$$\Delta p = -\rho_0 \frac{\partial u_i}{\partial x_j}\frac{\partial u_j}{\partial x_i}. \tag{3.4}$$

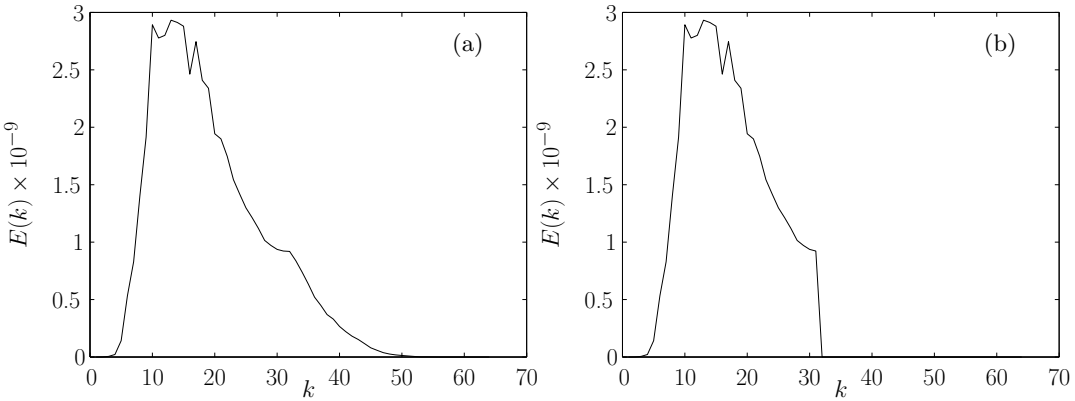

FIGURE 1. The energy spectrum of v. (a) original, (b) truncated.

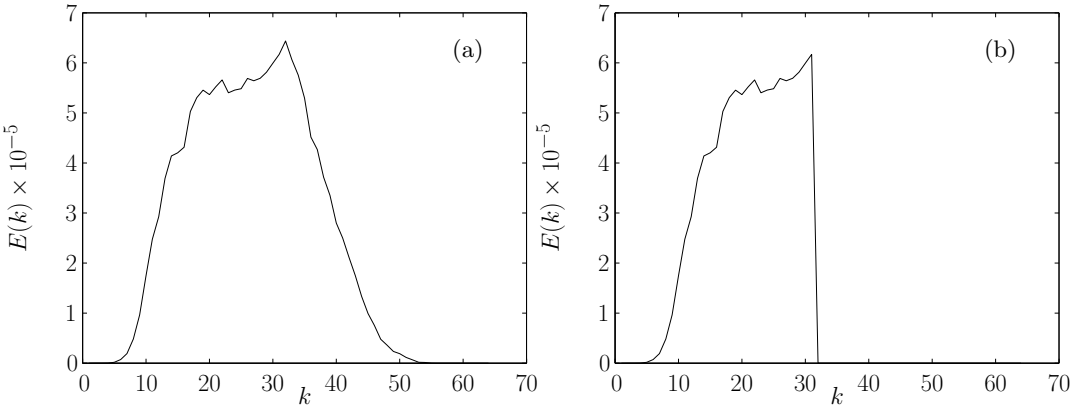

FIGURE 2. The energy of $v(t_1 + \Delta t) - v(t_1)$, (a) original, (b) truncated.

The initial density field is derived from the homentropic assumption as

$$\rho = (\gamma p)^{1/\gamma}. \tag{3.5}$$

Note that $\rho_0 = (2\pi)^{-3} \int_{\square} \rho \, \mathrm{d}V$. In the initial spectrum $k_0 = 4$ and $A = 5 \times 10^{-3}$ is taken such that, at $t = 0$, the turbulent Mach number is $M_t = u'/a_0 \approx 0.01$ and the Taylor-scale Reynolds number is $Re_T = u'\lambda/\nu \approx 80$.

The numerical experiments were performed on a series of 20 snapshots in time, separated by $\Delta t \approx 5 \times 10^{-2} L/a_0$, once the Taylor Reynolds number had dropped to 50. A typical three-dimensional energy spectrum of the velocity field v is given in Fig. 1(a). The velocity at $k = 31$ is Fourier-filtered to make it isotropic. The energy spectrum of the truncated velocity field v is given in Fig. 1(b). For two consecutive snapshots the energy decays by about 0.03%, as shown in Fig. 2.

3.3. *Numerical algorithm for the large-scale field U and for the first corrector u^1*

A Fourier spectral method is used to invert the Laplacian in the Poisson equation (2.19). All the nonlinear terms are computed in the real space, and all the derivatives are computed in the Fourier space. The Reynolds stress is found by computing (2.21) and then truncating to $k \leq 15$. The time integration of (2.7) is performed using the second order

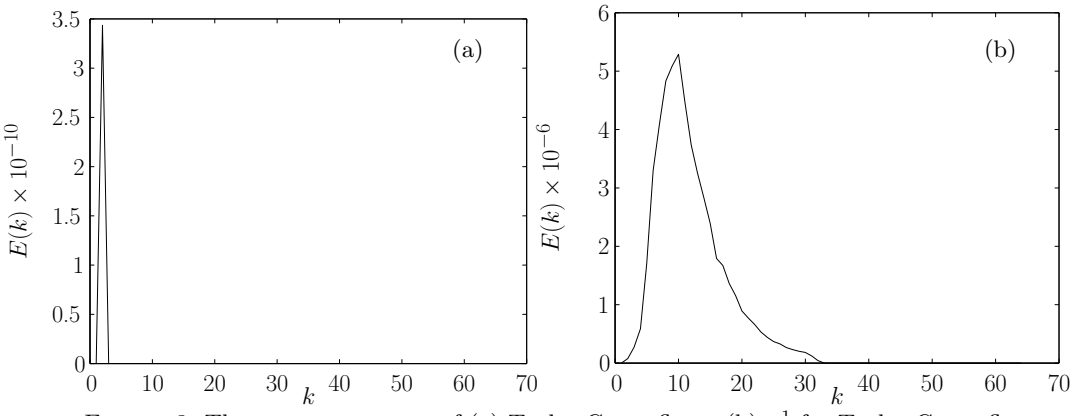

FIGURE 3. The energy spectrum of (a) Taylor-Green flows, (b) u^1 for Taylor-Green flows.

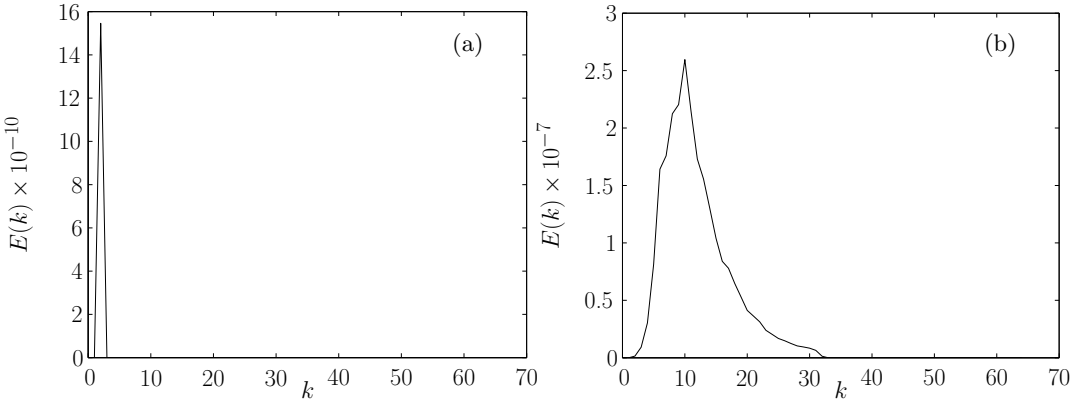

FIGURE 4. The energy spectrum of (a) ABC-flows, $A = 1$, $B = -1$, $C = .5$, (b) u^1 for ABC-flows.

Runge-Kutta method, in which the nonlinear term is computed explicitly in time and the linear term (Laplacian) is treated implicitly in time and in the Fourier space.

3.4. *Numerical verification of asymptotic expansions*

3.4.1. *The first corrector*

Numerically, the relative L_2-norm of the difference between the solution of (2.19) and (2.18) is less than 5%. Therefore, in the first approximation, $\partial u^1/\partial t$ can be neglected. Figure 5 shows the numerical validation of the final approximation between u^1 and $\tilde{u}^1$ that solve (2.19) and (2.20), respectively, for the present data. In Fig. 5(a) the spectrum of $\tilde{u}^1$ is shown, and in Fig. 5(b) is shown the spectrum of the difference $u^1 - \tilde{u}^1$. (Compare Fig. 5(a) with Fig. 3.) At small scales the approximation is reasonable.

3.4.2. *Reynolds stress*

To discuss the meaning of $\langle\cdot\rangle$, consider

$$\tau^1_{ij} = u^1_j v_i + v_j u^1_i \tag{3.6}$$

without the brackets $\langle\cdot\rangle$. For a given flow Taylor-Green- or ABC-flow U_o (with spectra in Figs. 3(a) and 4(a), respectively), the energy spectra of the τ^1_{ij} is depicted in Figs. 6

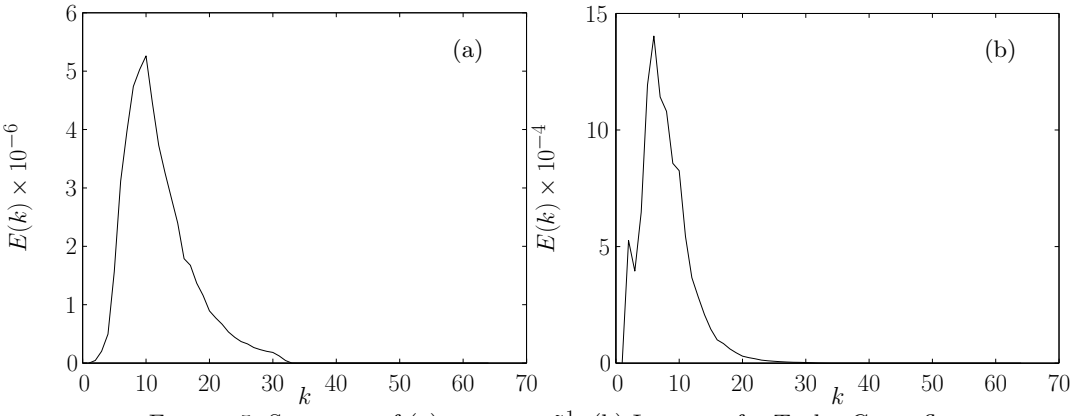

FIGURE 5. Spectrum of (a) corrector $\tilde{u}^1$, (b) Its error, for Taylor-Green flows.

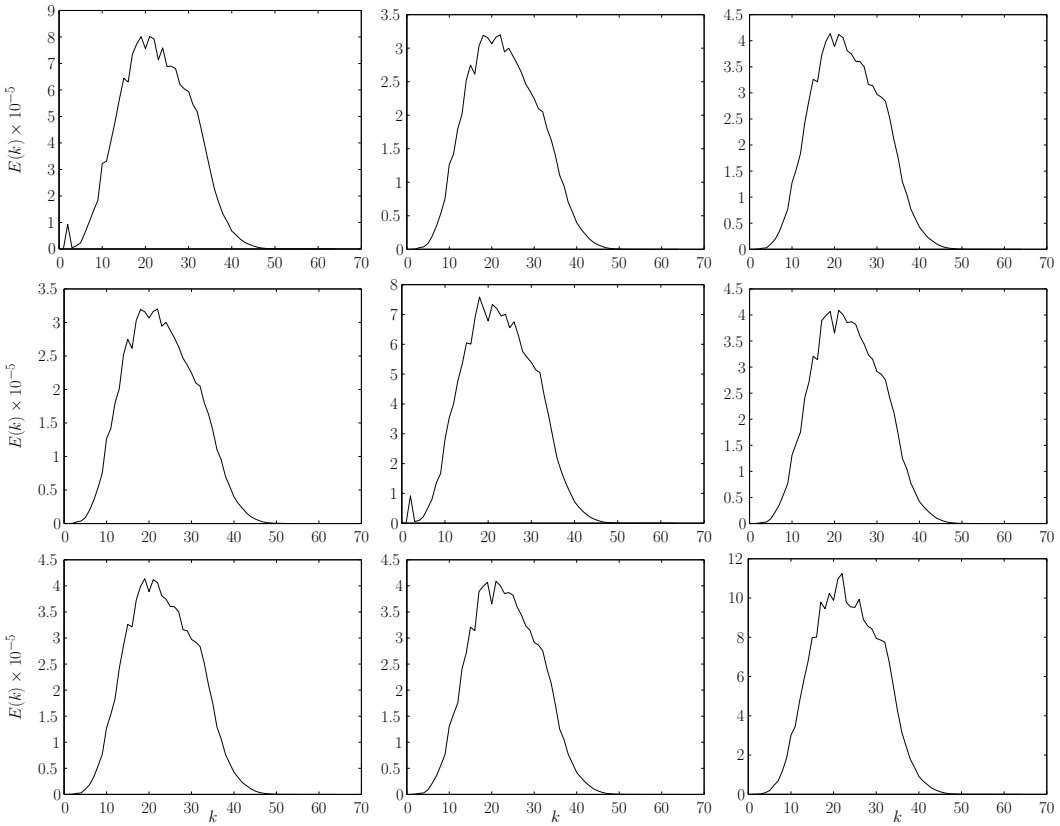

FIGURE 6. Spectrum of τ^1_{11}, τ^1_{12}, τ^1_{13} (first row, left to right), τ^1_{21}, τ^1_{22}, τ^1_{23} (second row), τ^1_{31}, τ^1_{32}, τ^1_{33} (third row) for Taylor-Green flows.

and 7, respectively. In each flow the spectra have two visible maxima: one at low k and the other at large k. The spectrum of τ^1_{ij} is projected onto the large-scale field with wavenumber $k \leq 15$. Hence, the fast-variable average $\langle\cdot\rangle$ projects the full-spectrum stress τ^1_{ij} onto the large-scale stress τ^o_{ij}.

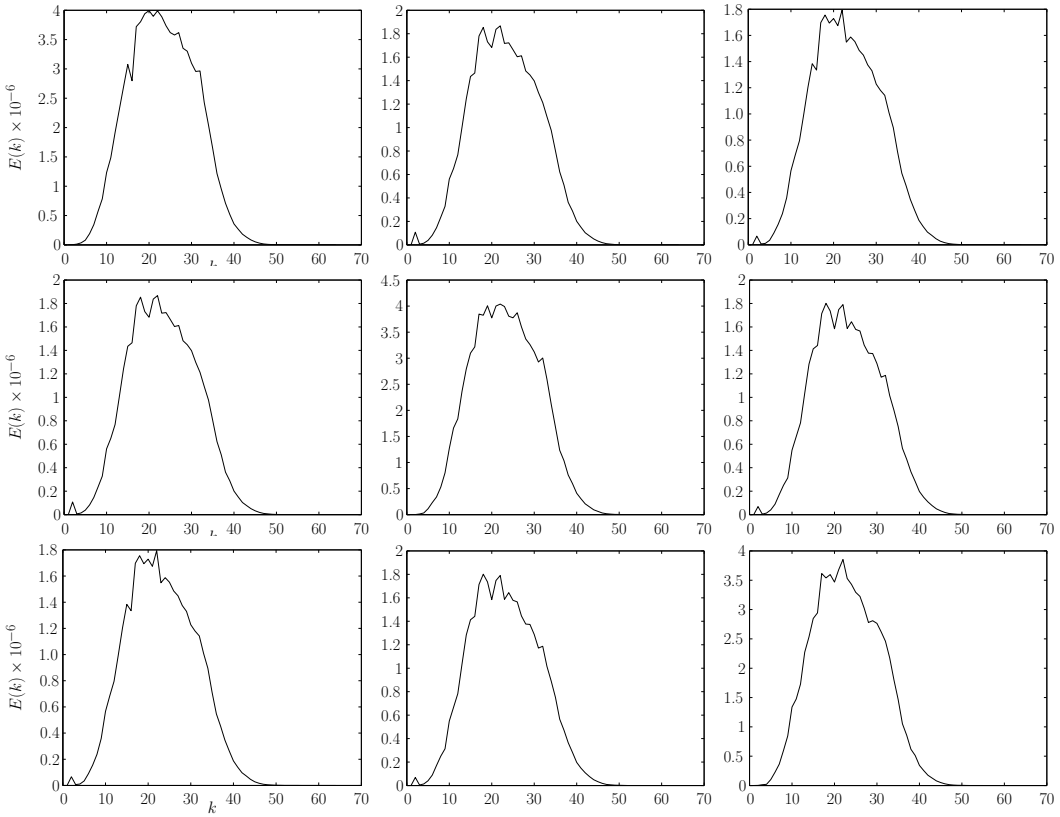

FIGURE 7. Spectrum of τ^1_{11}, τ^1_{12}, τ^1_{13} (first row, left to right), τ^1_{21}, τ^1_{22}, τ^1_{23} (second row), τ^1_{31}, τ^1_{32}, τ^1_{33} (third row) for ABC-flows.

The stress τ^o_{ij} is clearly a symmetric second degree tensor. In particular, comparison of Fig. 6 and Fig. 7 shows that the two visible maxima appear either for the diagonal entries of τ^1_{ij} or for its off-diagonal entries. Note that all τ^1_{ij} are a product of two small-scale flows only. In principle, their product may have no large-scale components, but in the present case it does, implying a net effect in the large-scale equation (2.7). A natural question is whether the presense of the pressure has any effect in removing the maxima at large scales. To answer this, the spectrum of the Leray-projected stress $\bar{\tau}^1_{ij}$ defined by

$$\bar{\tau}^1 = -\nabla \times \Delta^{-1}\mathbb{P}\left(\nabla \cdot \tau^1\right), \ \nabla\times = \begin{pmatrix} 0 & -\nabla_3 & \nabla_2 \\ \nabla_3 & 0 & -\nabla_1 \\ -\nabla_2 & \nabla_1 & 0 \end{pmatrix}$$

is plotted in Fig. 8. The maxima at large scales are clearly visible for both Taylor-Green flows and ABC-flows.

3.5. A priori *characterization of the model in decaying isotropic turbulence*

To apply the multiscale analysis to a particular flow, it must be defined what is meant by 'scale separation,' and a particular wavenumber (lengthscale) must be associated to the separation. In preparation for applying the analysis in a true LES context the assumption is made that for the isotropic turbulence under consideration a LES with 32^3 grid points would be typical. Hence the association of the wavenumber $k = 15$, which is one less

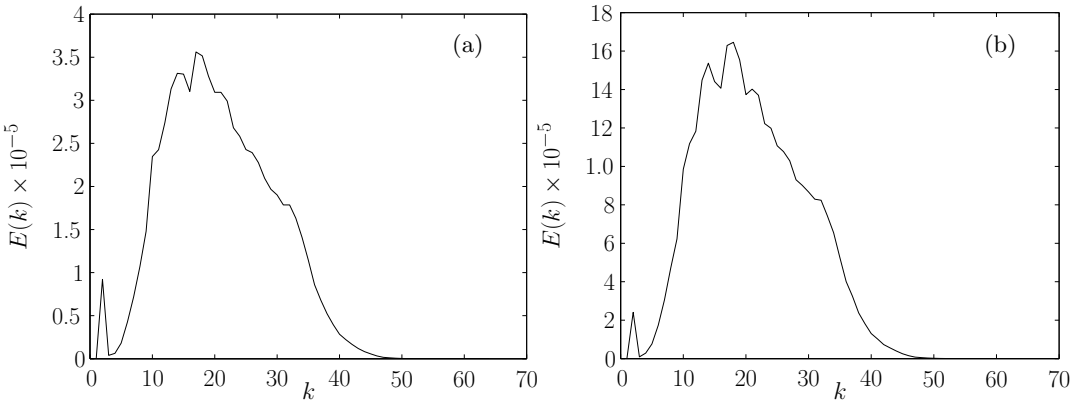

FIGURE 8. Spectrum of $\bar{\tau}$ (a) Taylor-Green flows, (b) ABC-flows

than the Nyquist wavenumber for the 32-point grid. This wavenumber, at its assocated length $2\pi/k$, defines the statement of 'small' and 'large.'

The first, and rather coarse, step in analyzing the relevance of this model is to assume that the eddy viscosity approximation is valid and to try to estimate the model's eddy viscosity. This is done in the Fourier space by appealing to the well known result that the three-dimensional turbulent kinetic energy spectrum satisfies the integro-differential equation

$$\frac{1}{2}\frac{\partial E}{\partial t} = T(k) - \nu|k|^2 E(k), \tag{3.7}$$

where $T(k)$ is the redistrubution integral involving wavenumber triplets and ν is the kinematic viscosity. $T(k)$ can be modelled through an effective wavenumber-dependent eddy viscosity such that

$$\frac{1}{2}\frac{\partial E}{\partial t} = -\nu_k^{\text{eff}}|k|^2 E(k). \tag{3.8}$$

In the case of decaying turbulence, it is expected that the value of the eddy viscosity should be isotropic with respect to space. Thus the eddy viscosity should be the same for any choice of constants A, B, C in (3.1) for ABC-flow, and it should be the same for any choice of δ in (3.2) for the cat's-eye flow. Table 1 shows the dependence of eddy viscosity on A, B, C for ABC-flows (3.1) and Table 2 shows the dependence of eddy viscosity on δ for cat's-eye flows (3.2). Within a class of flows, the effective eddy viscosity is independent of the large-scale flow orientation so that the response of the model is isotropic. This consistency check ensures that the multiscale description does not have a preferred direction. Note, however, that the effective eddy viscosity varies according to the large-scale field. Furthermore, the eddy viscosity responds to the total energy of the large-scale field, as evidenced in Fig. 9.

Figure 10 shows the distribution of ν^{eff} as a function of wavenumber k. There exists a peak value of the eddy viscosity, and for $k < 3$ the eddy viscosity becomes negative, thereby indicating that some backscatter is retained in the first corrector. For larger values of k, the eddy viscosity decreases but remains positive as $\nu^{\text{eff}} \to \nu$ as $k \to \infty$.

A	-1	-1	-1	-1	0	1
B	-1	-1	-1	0.5	2	2
C	-1	0	0.3	0.5	0.5	0.5
ν_1^{eff}	0.0330	0.0329	0.0328	0.0325	0.0328	0.0329

TABLE 1. Eddy viscosity of ABC-flows, taken at $t = t_2$

δ	0	0.1	0.2	0.3	0.4	0.5	0.6	0.7	0.8	0.9	1
$\nu_{\sqrt{2}}^{\text{eff}}$	0.0334	0.0334	0.0334	0.0334	0.0334	0.0335	0.0335	0.0335	0.0335	0.0335	0.0335

TABLE 2. Eddy viscosity of cat's-eye flows, taken at $t = t_2$

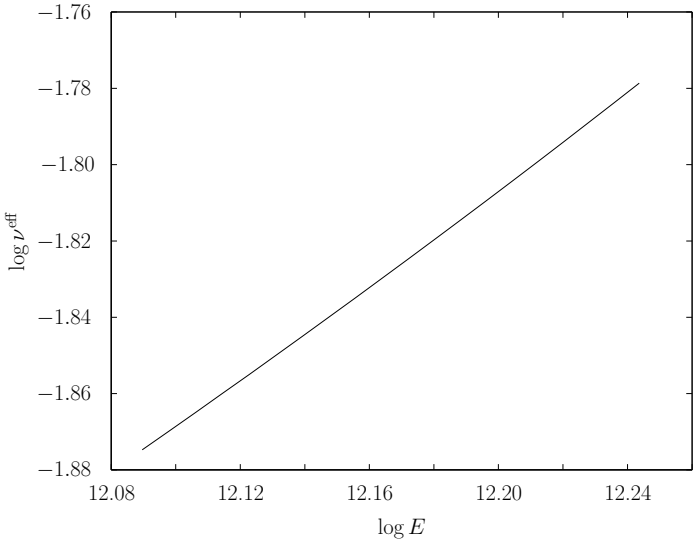

FIGURE 9. Eddy viscosity of ABC-flows as a function of energy of basic flow.

4. A posteriori characterization of the model in decaying isotropic turbulence

The relevance of the proposed approach to turbulence modeling relies on its ability to replicate the behavior of the unresolved stress on the resolved LES field without prescribing the SGS field. As a first attempt, a synthesized velocity field with a known spectrum is used. The model's response is then evaluated. To verify such synthetic data in the proposed framework, a comparison is performed on the results of numerical simulations when the SGS flow is given by the simulated data and when it is given by synthetic data. In this section the method is applied in a more realistic LES setting when the subgrid scale field is not known but instead must be estimated.

The synthesized velocity field v is constructed using the von Kármán-Kraichnan spec-

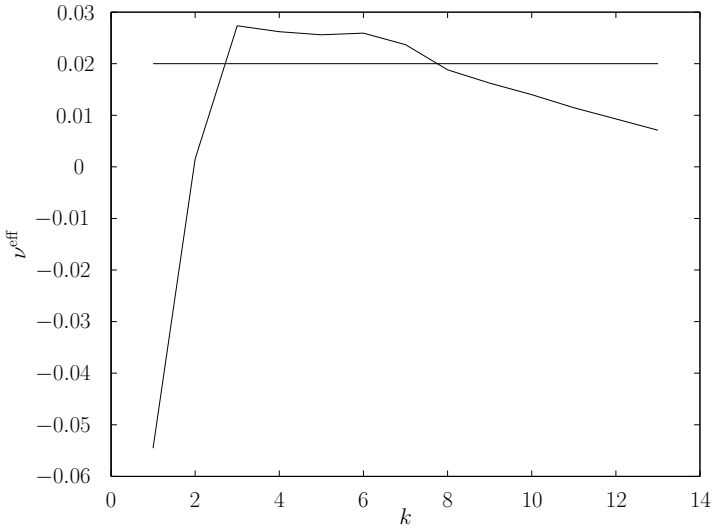

FIGURE 10. Eddy viscosity of turbulent flows for different wave-numbers

trum

$$E(k) = \frac{3}{2I_1}\frac{u'^2}{k_0}\frac{(k/k_0)^4}{(1+\frac{12}{5}(k/k_0)^2)^{17/6}}\exp\left\{-\beta Re_L^{-3/4}(k/k_0)\right\}, \tag{4.1}$$

where Re_L is the integral lengthscale-based Reynolds number, $\beta = 8.36$, and I_1 is evaluated at finite Reynolds number such that $\int_0^\infty E(k)\,\mathrm{d}k = (3/2)u'^2$. The spectrum constants k_0 and u'^2 are chosen such that $u'/a_0 = 0.01$ and the Taylor Reynolds number is approximately 50; these conditions approximately correspond to those used in the previous *a priori* analysis. Reconstruction of the solenoidal velocity field follows the procedure outlined above.

In Fig. 11 the comparison of the effective viscosity is shown for the synthesized velocity field against the direct numerical simulation data. In the figure the results of four numerical experiments are shown. In each case the large-scale flow taken from the DNS data with wavenumber $k \leq 7$ is the same and not from the Beltrami- or cat's eye flows used in the previous section. However, the SGS field (with wavenumber $k > 7$) is constructed

- to be identically zero, *i.e.*, no small scale field. This represents no model (Case 1).
- from the same DNS data (Case 2).
- from different realizations of DNS data (Cases 3a and 3b).
- from the synthesized data (Case 4).

In the figure the dashed curve represents the results of full DNS for the data and represents the reference data.

As can be seen in Fig. 11, the simulated data approximates the full DNS, supporting the expression for the unresolved stress of (2.21). Moreover, the replacement of the small scale flow from other realizations shows good consistency, suggesting that the formulation has some robustness to changes in phase of the velocity field. The synthesized data shows lower performance, especially at small wavenumbers, where the assumptions of the multiscale analysis no longer hold. However, it performs better than does the purely large-scale field.

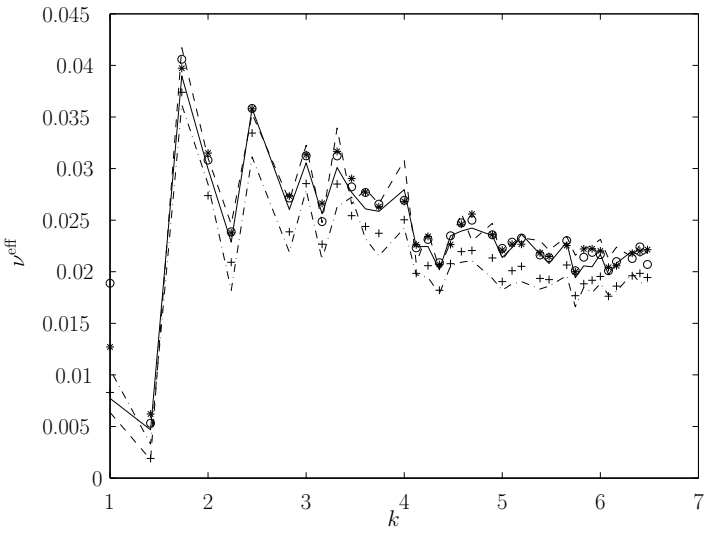

FIGURE 11. Comparison of effective viscosity for synthesized and simulated data. Legend: $--$ full DNS; $-\cdot-$ (Case 1, no SGS field); — (Case 2, DNS data); $\circ$, $*$ (Cases 3a and 3b, different realizations of DNS data); $+$, (Case 4, synthesized velocity field).

δ	0	0.1	0.2	0.3	0.4	0.5	0.6	0.7	0.8	0.9	1
Case 1	0.0200	0.0200	0.0200	0.0200	0.0200	0.0200	0.0200	0.0200	0.0200	0.0200	0.0200
Case 2	0.0230	0.0230	0.0230	0.0230	0.0231	0.0231	0.0231	0.0231	0.0231	0.0231	0.0231
Case 3a	0.0229	0.0230	0.0230	0.0230	0.0230	0.0231	0.0231	0.0231	0.0231	0.0231	0.0231
Case 3b	0.0228	0.0228	0.0228	0.0228	0.0228	0.0228	0.0228	0.0229	0.0229	0.0229	0.0229
Case 4	0.0202	0.0202	0.0202	0.0202	0.0202	0.0202	0.0202	0.0202	0.0202	0.0202	0.0202

TABLE 3. Summary of the effective viscosity $\nu^{\rm eff}_{\sqrt{2}}$ for decaying isotropic turbulence.

5. Conclusions and future work

Through a multiscale, asymptotic analysis, an approximate expression (2.21) for the subgrid scale stress tensor τ has been derived. This expression has been evaluated against direct numerical simulation data of decaying isotropic turbulence. It was found that the expression preserves isotropy and permits backscatter in the context of an effective eddy viscosity. The expression was tested using a synthesized velocity field to determine the expression's performance, and it was found to produce reasonable estimates of the subgrid scale stresses without requiring any modeling coefficients.

It is apparent that this approach has some potential but needs further consideration. In tests on direct numerical simulation data of a fully developed turbulent channel flow (not described here), the model exhibited anisotropic response and increased sensitivity near the channel walls. A need exists for the introduction of a modeling coefficient so that the unresolved stress is more sensitive to the large scale field.

Acknowledgments

A.N. was supported by the Center for Turbulence Research during the summer of 2005. He thanks Parviz Moin for his hospitality. He also thanks Jeremy Templeton and Javier Jimenez for illuminating discussions.

REFERENCES

Bardina, J., Ferziger J. H., & Reynolds, W. C. 1980 Improved subgrid scale models for large-eddy simulation. *AIAA-80-1357*.

Batchelor, G. K. 1953 *The Theory of Homogeneous Turbulence*. Cambridge University Press.

Bensoussan, A., Lions, J.-L. & Papanicolaou, G. 1978 *Asymptotic Analysis for Periodic Structures,* North-Holland.

Blaisdell, G. A., Mansour N. N., & Reynolds W. C. 1991 Numerical simulations of compressible homogeneous turbulence, Thermosciences *Report TF-50*, Stanford University.

Bodony, D. J. & Lele, S. K. 2002 Spatial scale decomposition of shear layer turbulence and the sound sources associated with the missing scales in a large-eddy simulation. *AIAA-2002-2454*.

Cabot, W. H., Schilling, O. & Zhou Y. 2004 Influence of subgrid scales on resolvable turbulence and mixing in Rayleigh-Taylor flow, *Phys. Fluids* **16**, 495–508.

Constantin, P. & Foias, C. 1988 Navier-Stokes equations. *Chicago Lectures in Mathematics*. University of Chicago Press.

Debussche, A., Dubois, T., & Temam, R. 1993 The nonlinear galerkin method: a multi-scale method applied to the simulation of homogeneous turbulent flows. *ICASE Report 93-93*, ICASE/NASA Langley Research Center.

Dubrulle, B. & Frisch, U. 1991 Eddy viscosity of parity-invariant flows, *Phys. Rev. A* **43**, 5355–5364.

Dubrulle, B., Laval, J.-P., Nazarenko, S., & Kevlahan, N. K.-R. 2001 A dynamic subfilter-scale model for plane parallel flows, *Phys. Fluids* **13**, 2045-2064.

Frisch, U. 1995 *Turbulence. The legacy of A. N. Kolmogorov*. Cambridge University Press.

Germano, M., Piomelli, U., Moin, P., & Cabot, W. H. 1991 A dynamic subgrid-scale eddy viscosity model. *Phys Fluids A* **3**, 1760–1765.

Kolmogorov, A. N. 1941 Local structure of turbulence in incompressible viscous flow for very large Reynolds number. *Doklady Akademiya Nauk SSSR*. **30**, 299–303.

Laval, J.-P., Dubrulle, B. & Nazarenko, S. 2000 Dynamical modeling of sub-grid scales in 2D turbulence, *Physica D* **142**, 231-353.

Meneveau, C. 1991 Analysis of turbulence in the orthonormal wavelet representation. *J. Fluid Mech.* **232**, 496–512.

Meneveau, C. & Katz J. 2000 Scale-invariance and turbulence models for large-eddy simulation, *Ann. Rev. Fluid Mech.* **32**, 1–32.

Novikov, A. 2003 Modulational stability of cellular flows, *Nonlinearity* **16**, 1607–1639.

Novikov, A. 2004 Eddy viscosity of cellular flows by upscaling, *J. Comp. Phys.* **195**, 341–354.

Novikov, A. & Papanicolaou, G. 2001 Eddy viscosity of cellular flows, *J. Fluid Mech.* **446**, 173-198.

Sivashinsky, G. I. 1985 Weak turbulence in periodic flows, *Physica D* **17**, 243–255.

Sivashinsky, G.I. & Frenkel, A.L. 1992 On negative eddy viscosity under conditions of isotropy, *Phys. Fluids A* **4**, 1608–1610.

Sivashinsky, G.I. & Yakhot, V. 1985 Negative viscosity effect in large-scale flows, *Phys. Fluids* **28**, 1040–1042.

Smagorinsky, J. 1963 General circulation experiments with the primitive equations. I. The basic experiment. *Mon. Weather Rev.* **91**, 99–164.

Zimin, V. & Hussain, F. 1995 Wavelet based model for small-scale turbulence, *Phys. Fluids* **7**, 2925–2927.